Cell Metabolism
Article

Nuclear Receptor Corepressor SMRT Regulates Mitochondrial Oxidative Metabolism and Mediates Aging-Related Metabolic Deterioration

Shannon M. Reilly,[1] Prerna Bhargava,[1] Sihao Liu,[1] Matthew R. Gangl,[1] Cem Gorgun,[1] Russell R. Nofsinger,[3,4] Ronald M. Evans,[3] Lu Qi,[2] Frank B. Hu,[2] and Chih-Hao Lee[1,2,*]
[1]Department of Genetics and Complex Diseases
[2]Department of Nutrition
Division of Biological Sciences, Harvard School of Public Health, 665 Huntington Avenue, Boston, MA 02115, USA
[3]Gene Expression Laboratory, Howard Hughes Medical Institute at the Salk Institute for Biological Studies, 10010 North Torrey Pines Road, La Jolla, CA 92037, USA
[4]Present address: Illumina, Inc., 9885 Towne Centre Drive, San Diego, CA 92121, USA
*Correspondence: clee@hsph.harvard.edu
DOI 10.1016/j.cmet.2010.11.007

SUMMARY

The transcriptional corepressor SMRT utilizes two major receptor-interacting domains (RID1 and RID2) to mediate nuclear receptor (NR) signaling through epigenetic modification. The physiological significance of such interaction remains unclear. We find SMRT expression and its occupancy on peroxisome proliferator-activated receptor (PPAR) target gene promoters are increased with age in major metabolic tissues. Genetic manipulations to selectively disable RID1 ($SMRT^{mRID1}$) demonstrate that shifting SMRT repression to RID2-associated NRs, notably PPARs, causes premature aging and related metabolic diseases accompanied by reduced mitochondrial function and antioxidant gene expression. $SMRT^{mRID1}$ cells exhibit increased susceptibility to oxidative damage, which could be rescued by PPAR activation or antioxidant treatment. In concert, several human *Smrt* gene polymorphisms are found to nominally associate with type 2 diabetes and adiponectin levels. These data uncover a role for SMRT in mitochondrial oxidative metabolism and the aging process, which may serve as a drug target to improve health span.

INTRODUCTION

Aging and metabolic diseases share certain common pathogeneses. Caloric excess results in metabolic diseases and shorter life expectancy. Conversely, caloric restriction (CR) improves metabolic parameters and increases longevity (Lee et al., 2009; Murphy et al., 2003). At the cellular level, the age-dependent decline in mitochondrial function has been implicated in aging and related metabolic disorders (Balaban et al., 2005; Reznick et al., 2007; Zid et al., 2009). The electron transport chain drives the oxidative phosphorylation (OXPHOS) of ADP to produce ATP. An unavoidable by-product of mitochondrial respiration is the generation of reactive oxygen species (ROS). Many cellular mechanisms exist to protect the cell and its organelles from oxidative damage (Wallace and Fan, 2009). ROS scavenging proteins, including superoxide dismutase 1 (SOD1), SOD2, glutathione peroxidase (GPx), catalase, and glutathione S-transferases pi (GSTP), possess enzymatic functions that neutralize specific ROS. If uncontrolled, oxidative damage caused by ROS affects proteins, lipids, and nucleic acids, leading to enzyme and membrane dysfunctions as well as genetic mutations. These changes further reduce mitochondrial function and increase susceptibility of cells to oxidative stress, which is a hallmark of aging (Kapahi et al., 1999; Kenyon, 2005). ROS have also been implicated in the pathogenesis of metabolic diseases (Roberts and Sindhu, 2009), while treatment with small antioxidant molecules improved glucose handling and insulin sensitivity (Houstis et al., 2006).

Several signaling pathways have been linked to both life span and metabolic homeostasis. Sir2, a member of the sirtuin family of NAD-dependent deacetylases, is one of the signaling proteins attributed to the beneficial effects of CR (Guarente, 2006). Resveratrol activates the mammalian homolog of Sir2, SIRT1, to improve longevity and protect mice from the metabolic disturbances caused by high-fat-diet-induced obesity (Baur et al., 2006; Lagouge et al., 2006). The effects of SIRT1 on metabolism are mediated in part by PPARγ coactivator-1α (PGC-1α), which is activated through deacetylation by SIRT1 (Rodgers et al., 2005). Although not directly implicated in longevity, PGC-1α has been shown to promote the expression of ROS scavenger proteins, thereby preventing neurodegeneration (St-Pierre et al., 2006). PGC-1α also regulates genes involved in oxidative metabolism and mitochondrial biogenesis by activating transcription factors (Lin et al., 2005), including PPARs. The PPAR nuclear receptor (NR) family consists of PPARα, PPARδ (also called PPARβ), and PPARγ, all of which are drug targets for components of metabolic syndrome (Lee et al., 2003; Reilly and Lee, 2008). PPARα and PPARγ exhibit more restricted effects on fatty acid β oxidation and fat storage in the liver and adipocyte, respectively. PPARδ has a broad tissue expression pattern and has been shown to regulate fat catabolism and OXPHOS in muscle, brown adipose tissue (BAT), and macrophages (Kang et al., 2008; Pan et al., 2009; Wang et al., 2004).

The transcriptional activities of PPARs and many other NRs on target gene expression are modulated by coactivator and corepressor complexes through epigenetic modifications (Glass and Rosenfeld, 2000). Coactivators, such as PGC-1α, recruit the p300 family of histone acetyltransferases to ligand-activated NRs to promote target gene expression. Reciprocally, unliganded NRs interact with corepressor complexes containing histone deacetylases (HDACs), which inhibit transcription. Silencing mediator of retinoid and thyroid hormone receptors (SMRT) and nuclear receptor corepressor (N-CoR) are the two major corepressors that regulate the activity of many transcription factors (Privalsky, 2004). These two proteins are structurally similar, containing two major nuclear receptor-interacting domains (RID1 and RID2). Biochemical analyses have identified the IXXI(V)I sequence within RIDs, termed the CoRNR box motif, which provides the interface for NR/corepressor interaction (Glass and Rosenfeld, 2000). These two RIDs preferentially interact with different NR groups. For example, retinoic acid receptors (RARs) associate with RID1, while most lipid-sensing receptors, including PPARs and retinoid X receptors (RXRs), utilize RID2 located at the C terminus (Hu et al., 2001). Alternative splicing events have been identified within this RID-containing region, resulting in several splice variants, including one isoform with an additional, third RID domain, which enhances thyroid hormone receptor (TR) interaction (Cohen et al., 2001), and one without RID2. These observations indicate that each RID has specific functions through recruitment of distinct sets of NRs. Given the role of corepressors in NR-mediated transcription, we sought to examine whether they are involved in suppression of NR activity in pathological conditions. We were particularly interested in the function of RID2, which recruits PPARs and other lipid-sensing receptors. Consequently, we have obtained a knockin mouse model that selectively disables RID1. The mutant SMRT will mainly function as a corepressor for RID2-associated NRs. Our results show that shifting SMRT repression to RID2 leads to inhibited PPAR activity and depressed OXPHOS and mitochondrial function. The data also reveal a role for SMRT in aging and the related metabolic disorders.

RESULTS

A Genetic Model to Study the Role of SMRT in Metabolic Regulation

We found that SMRT mRNA and protein levels were induced in BAT and muscle from older mice, independent of high-fat-diet feeding (Figures 1A and S1B, 2-month-old versus 6-month-old). SMRT protein, but not mRNA, was also elevated in white adipose tissue (WAT) with age. We hypothesized that SMRT may be involved in processes of age-related metabolic diseases. Accordingly, a genetic model designated as SMRT^{mRID1}, in which the conserved amino acids of the CoRNR box in SMRT RID1 were mutated to alanine (IXXVI to AXXAA) (Figure 1B), was studied. The complete description of the generation of this mouse model will be reported elsewhere. The resultant SMRT protein is expected to associate only with RID2-interacting receptors, including PPARs, which are known regulators of mitochondrial oxidative metabolism. SMRT^{mRID1} mice were born in normal Mendelian ratios. The expression of SMRT and N-CoR was not altered in these mice (Figures S1D and S1E). The SMRT C-terminal regions with WT RID1/2 (RID1 + RID2) (Figure 1B, bottom panel), mutant RID1 and WT RID2 (mRID1 + RID2 from SMRT^{mRID1} mice), or a natural splice variant containing only RID1 (RID1) were placed downstream of GAL4-DNA-binding domain (GAL4-DBD) for testing interaction against receptor ligand-binding domains (LBD) fused to VP16 activation domain in the mammalian two-hybrid (M2) system (Figure 1C, top panel). It has been shown that RARs interact primarily with SMRT RID1, whereas TRs and PPARs interact predominantly with SMRT RID2. The M2 interaction assay confirmed that the association between RARα and SMRT was reduced by the RID1 mutation and that TRα interacted equally well with RID1 + RID2 and mRID1 + RID2 (Figure 1C). Intriguingly, the interaction of mRID1 + RID2 with PPARs was greater than that of WT RIDs, likely because in the absence of RID1-associated NR binding, RID2 becomes more readily available to bind PPARs (Figure 1D). In line with this, the untagged WT PPARδ competed more efficiently with VP16-RARα for interaction with GAL4-mRID1 + RID2 than GAL4-RID1 + RID2 (Figure 1E). PPARδ was used here and in later experiments, as it is expressed in most tissues/cell types. The decreased and increased affinity of mRID1 + RID2 for RAR and PPAR, respectively, could also be observed with DNA-bound RAR/RXR and PPAR/RXR complexes in gel shift assays (Figure S1F). In addition, we found that while GAL4-N-CoR RID1 + RID2 interacted equally well with VP16-PPARδ and VP16-RARα, GAL4-SMRT RID1 + RID2 appeared to interact more strongly with VP16-PPARδ (Figure 1F), indicating that SMRT may be more relevant for PPAR function compared to N-CoR. Another important metabolic regulator, LXRα, showed stronger interaction with N-CoR, whereas LXRβ associated weakly with both SMRT and N-CoR (Figure 1G), as reported previously (Hu et al., 2003). The interaction between LXRα/β and mRID1 + RID2 was unaltered. These data suggest that SMRT^{mRID1} may serve as a model to examine the effect of increased SMRT repression on activities of NRs, notably the PPARs, a scenario likely to occur in conditions of metabolic dysregulation associated with aging when SMRT expression is upregulated. Subsequently, SMRT^{mRID1} were bred into the C57BL/6 background, which is more suitable for metabolic studies.

SMRT^{mRID1} Mice Develop Premature Aging and Related Metabolic Diseases

Although born at the same weight as their WT littermates, both female and male SMRT^{mRID1} mice gained significantly more body weight with age on chow diet (Figures 2A and S2A). Six-month-old female SMRT^{mRID1} mice showed higher percentage body fat and decreased lean mass, as determined by dual-energy X-ray absorptiometry (DEXA) scanning (Figure 2B). DEXA also revealed that the bone mineral density was reduced in SMRT^{mRID1} mice (Figure 2C). In older animals, SMRT^{mRID1} mice developed cataracts, alopecia, and gray hair sooner than WT controls (Figures 2D and 2E). In addition, the rotarod test demonstrated that SMRT^{mRID1} mice had diminished sensorimotor coordination (Figure 2F), implicating a premature aging phenotype. Accordingly, cohorts of male and female mice fed ad libitum were allowed to age and die of natural causes to determine life expectancy. Kaplan-Meier survival curves showed that both female ($p = 0.028$) and male ($p = 0.012$) SMRT^{mRID1} mice had shortened life span (Figure 2G). To determine whether

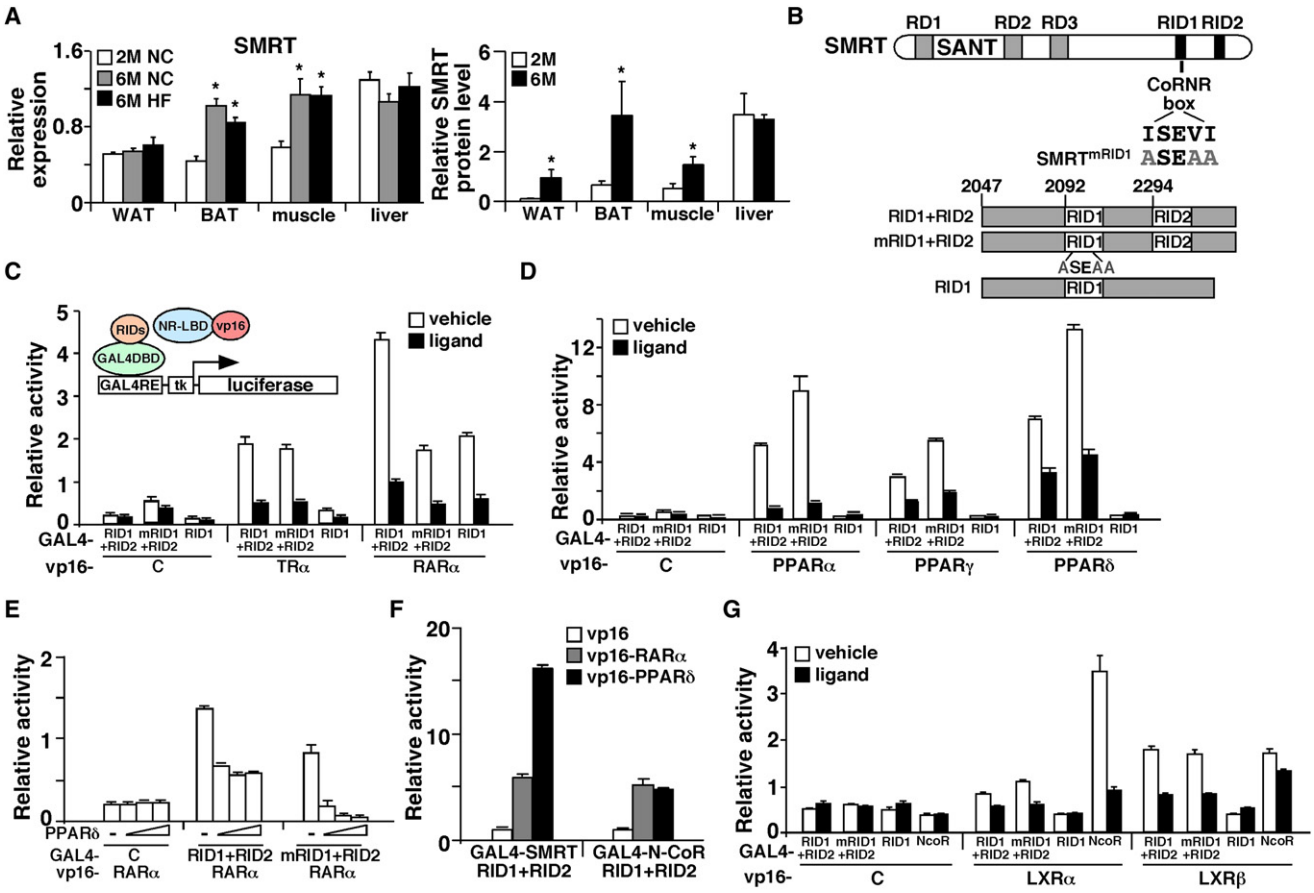

Figure 1. Characterization of SMRT^{mRID1} Mutant

(A) Age-dependent upregulation of SMRT expression. Left: Tissue RNA samples (n = 6/group) were isolated from 2-month-old normal chow (2M NC), 6-month-old normal chow (6M NC), and 6-month-old high-fat-fed (6M HF) C56BL/6 male mice. The expression of *Smrt* was determined by real-time PCR. Right: SMRT protein was immunoprecipitated from 2- and 6-month-old tissues, quantified by western blotting, and normalized to actin signal of the inputs (see also Figure S1). *$p < 0.05$, comparing 6-month-old to 2-month-old.

(B) Generation of SMRT^{mRID1} mice. Top: Diagram showing the domain structure of SMRT. In SMRT^{mRID1}, the ISEVI motif in the CoRNR box of RID1 has been mutated to ASEAA. RD1–3, repression domains 1–3; RID, nuclear receptor-interacting domain. Bottom: The C-terminal regions of SMRT containing the two major RIDs from WT (RID1 + RID2) and SMRT^{mRID1} mice (mRID1 + RID2) as well as a splice variant lacking RID2 (RID1) were cloned into an expression vector downstream of GAL4-DNA-binding domain (DBD) for interaction assays.

(C and D) Mammalian two-hybrid assays to quantify SMRT^{mRID1} and NR interaction. GAL4-DBD-SMRT RID constructs shown in (B) were cotransfected with the ligand-binding domain (LBD) from various nuclear receptors fused to VP16 transactivation domain into AD293 cells, together with a luciferase reporter containing GAL4-binding sites and a renilla luciferase internal control. VP16 alone was included for control.

(E) A competition assay showing PPARδ competes more efficiently with VP16-RARα for interaction with SMRT^{mRID1} than WT SMRT. Increasing amounts of untagged PPARδ were cotransfected to determine the ability of PPARδ to reduce GAL4-RID/VP16-RARα interaction.

(F) PPARδ preferentially interacts with SMRT over N-CoR, demonstrated by mammalian two-hybrid assays.

(G) Mammalian two-hybrid assays to quantify LXR interaction with WT SMRT, SMRT^{mRID1}, and N-CoR. Values are expressed as means ± SEM. Ligand concentrations: T_3, 100 nM; all-*trans* retinoic acid, 100 nM; GW7647 (PPARα), 1 μM; GW1929 (PPARγ), 1 μM; GW501516 (PPARδ), 0.1 μM; T0901317 (LXRα/β), 1 μM.

SMRT^{mRID1} mice developed age-related metabolic diseases, metabolic studies were conducted in 6-month-old female cohorts on chow diet. Similar results were found in male SMRT^{mRID1} mice (Figure S2). SMRT^{mRID1} mice had elevated levels of fasting serum triglycerides, cholesterol, glucose, insulin, and leptin as well as reduced adiponectin concentrations compared to control animals (Figures 3A–3C). Corticosterone levels were not significantly different. Glucose tolerance tests (GTT) and insulin tolerance tests (ITT) were performed to further characterize the insulin sensitivity. Throughout GTT, serum glucose was higher in SMRT^{mRID1} mice than in WT mice (Figure 3D), which was consistent with increased glucose production in primary hepatocytes (Figure S2E). ITT showed that SMRT^{mRID1} mice were more insulin resistant (Figure 3E). Furthermore, insulin-stimulated p-Akt was reduced in SMRT^{mRID1} muscle (Figure 3F, no significant difference in adipose tissue and liver, data not shown). Muscle glucose transporter 4 (GLUT4) levels were also reduced (Figure 3G). These defects led to blunted insulin-induced glucose uptake in isolated soleus muscle from SMRT^{mRID1} mice. These findings demonstrate that SMRT^{mRID1} mice develop the metabolic syndrome, including hyperlipidemia and insulin resistance.

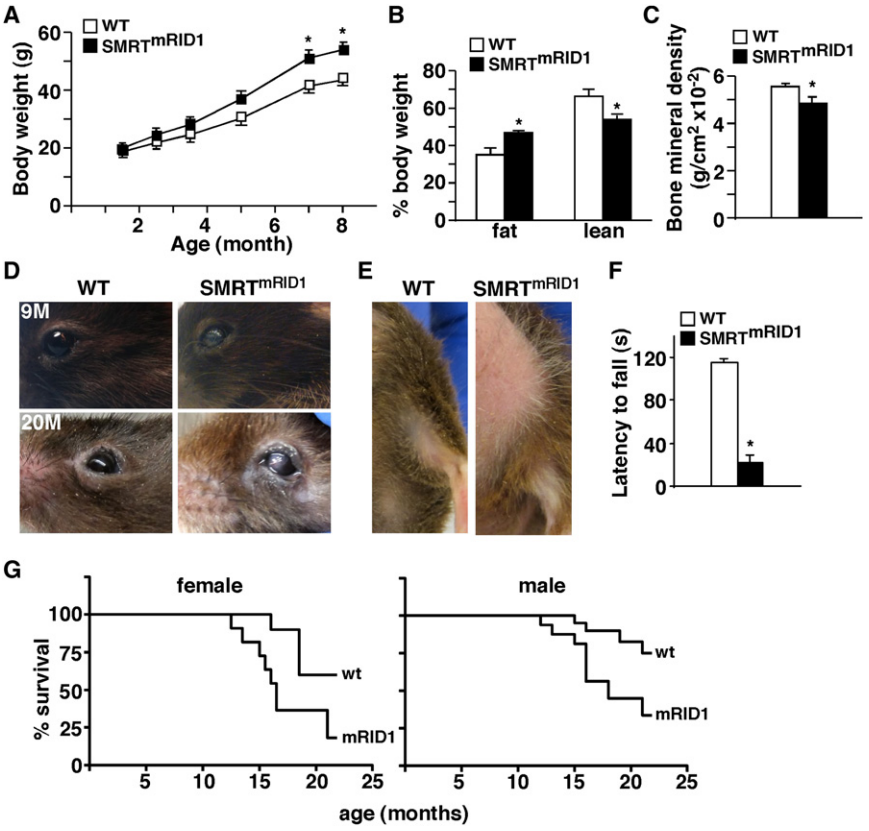

Figure 2. SMRT^{mRID1} Mice Show Premature Aging Phenotypes

(A) SMRT^{mRID1} female mice gain more weight on chow diet (n = 10/genotype).

(B and C) Body composition and bone mineral density determined by DEXA in 6-month-old female mice.

(D) The cataract phenotype in SMRT^{mRID1} mice. 9M, 9 months old; 20M: 20 months old.

(E) SMRT^{mRID1} mice (20 months old) exhibit alopecia in abdominal and lower back areas. The image also demonstrates hair graying.

(F) Rotarod test to examine sensorimotor coordination in 6-month-old female mice (n = 4/genotype).

(G) SMRT^{mRID1} mice have shortened life span. Cohorts of female and male mice (n = 20/genotype) on normal chow were allowed to age and die of natural causes to determine life expectancy using Kaplan-Meier survival curves. Values are expressed as means ± SEM. *p < 0.05, comparing WT to SMRT^{mRID1} mice.

PPAR Signaling Pathways Are Suppressed in SMRT^{mRID1} Mice

To identify metabolic pathways disturbed in SMRT^{mRID1} mice, gene expression analyses were performed. In BAT from SMRT^{mRID1} mice, the expression of medium-chain acyl-CoA dehydrogenase (*Mcad*), uncoupling protein-3 (*Ucp-3*), *Cidea* (a BAT marker), and several genes in the OXPHOS pathway was downregulated compared to control animals (Figure 4A). Levels of *Pparδ* and *Errα*, two NRs known to regulate oxidative metabolism, were also reduced. A similar reduction in genes encoding fatty acid oxidation and OXPHOS together with *Pparα*, a main regulator of hepatic lipid metabolism, was observed in the liver of SMRT^{mRID1} mice compared to control animals (Figure 4B). In contrast, the level of *Cyp26a1*, an RAR target gene, was increased. In WAT, in addition to fatty acid oxidation and OXPHOS genes, the expression of *Pparγ* and its targets, *Ap2* and *Adiponectin*, was decreased in SMRT^{mRID1} mice (Figure 4C). *Leptin* expression was not changed. The elevated circulating leptin was likely due to increased total fat mass. In muscle, OXPHOS genes were suppressed (Figure 4D). There was a reduction in *Glut4*, although it was not statistically significant. These data suggested that PPAR signaling pathways were suppressed in SMRT^{mRID1} mice. In fact, both basal activity and ligand activation of all three PPARs (GAL4-DBD-PPAR-LBD constructs) were reduced in SMRT^{mRID1} preadipocytes/fibroblasts (Figure 5A). To assess PPAR activity on target genes, chromatin immunoprecipitation (ChIP) of the endogenous *Mcad* gene was conducted using antibody against SMRT and IgG as a control in primary mouse embryonic fibroblasts (MEFs). *Mcad* was used, since it is a well-defined PPAR target (Gulick et al., 1994), and its expression was downregulated in multiple tissues in SMRT^{mRID1} mice. The expression of *Mcad* gene was reduced in SMRT^{mRID1} MEFs ± PPARδ ligand (Figure 5B, insert), which was associated with an increase in SMRT occupancy of the PPAR response element (PPRE) on *Mcad* promoter (Figure 5B). Similarly, SMRT occupancy on *Mcad* PPRE was significantly higher in BAT and the liver of SMRT^{mRID1} mice compared to control animals (Figure 5C). In contrast, SMRT binding to the RAR response element (RARE) of *Cyp26a1*was reduced, which was consistent with the in vitro M2 interaction results (Figures 1C and 1D). To probe the relevance of the current SMRT^{mRID1} model to the aging process, we compared SMRT ChIP in tissues from 2- and 6-month-old WT mice and found increased and decreased SMRT occupancy on *Mcad* PPRE and *Cyp26a1* RARE, respectively, in 6-month-old BATs and livers (Figure 5D). Thus, SMRT^{mRID1} mimics the age-dependent modulation of SMRT activity. These observations suggest that SMRT^{mRID1} suppresses the expression of genes encoding fatty acid catabolism and oxidative metabolism in part through inhibition of PPAR transcriptional activities. In addition, increased SMRT repression may contribute to the reduction in mitochondrial OXPHOS capacity in aged individuals.

Reduced Mitochondrial Function in SMRT^{mRID1} Mice

To determine whether the altered gene expression pattern has functional consequences, fatty acid β oxidation assays were conducted in BAT organ culture and in primary cells using radioactive tracers. We observed a 3-fold decrease in the rate of β oxidation in BAT of SMRT^{mRID1} mice compared to that of control animals (Figure 6A). Reduced fatty acid oxidation was also observed in hepatocytes and preadipocytes isolated from SMRT^{mRID1} mice. Furthermore, the ratio of mitochondrial DNA

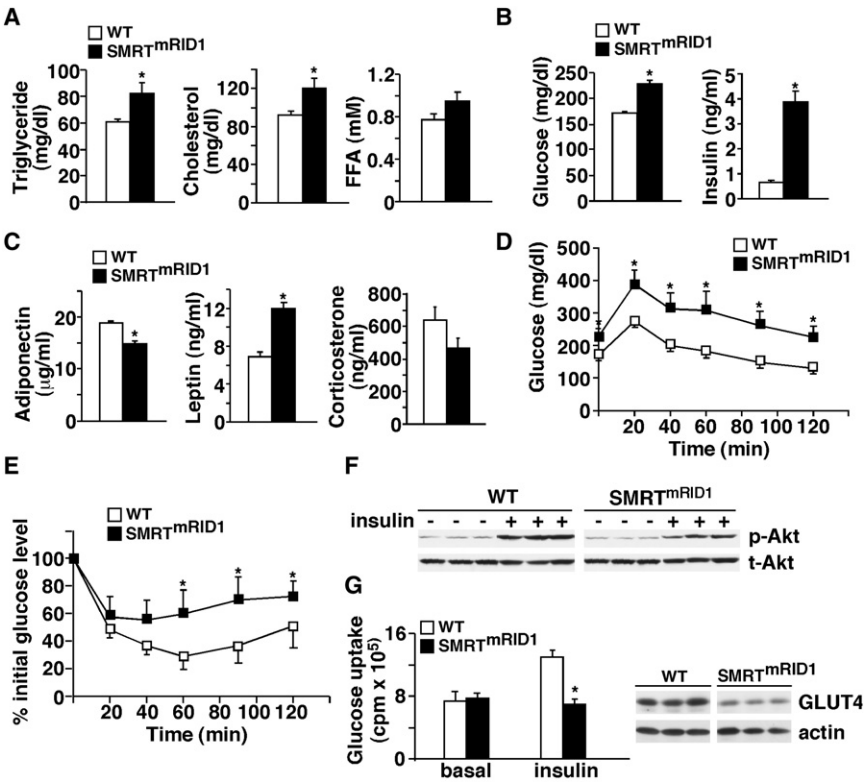

Figure 3. SMRT^{mRID1} Mice Develop Metabolic Diseases

(A–C) Blood chemistry analyses of fasting lipids, glucose, insulin, and adipokine levels in 6-month-old female mice (n = 7/genotype) on chow diet.

(D and E) Glucose tolerance test and insulin tolerance test. Mice were fasted 5 hr before the experiments.

(F) SMRT^{mRID1} mice exhibit reduced insulin sensitivity in muscle. Insulin signaling in muscle was determined by insulin-stimulated phospho-Akt (p-Akt). Mice (n = 5/genotype, showing representative samples from 3 individual mice) were i.p. injected with PBS or insulin (2 U/kg body weight). Muscle samples were collected 15 min later and analyzed by western blotting. The level of total Akt (t-Akt) was included for loading control.

(G) Insulin-stimulated glucose uptake conducted in soleus muscle using radioactive 2-deoxy-D-glucose. Right: Western blotting showing GLUT4 protein levels in muscle from 3 individual mice/genotype. Values are expressed as means ± SEM. *p < 0.05, comparing WT to SMRT^{mRID1} mice. Male mice showed similar phenotypes (Figure S2).

to nuclear DNA content was reduced in SMRT^{mRID1} muscle and BAT, indicating reduced mitochondrial number in these tissues (Figure 6B). Similarly, SMRT^{mRID1} MEFs had reduced mitochondrial staining by MitoTracker probes (Figure 6C). These results suggested that the metabolic phenotype of SMRT^{mRID1} mice was caused by reduced fat-burning capacity and compromised mitochondrial oxidative metabolism. In fact, using metabolic cages, we determined that SMRT^{mRID1} mice consumed less oxygen than WT mice (Figure 6D). They also exhibited a lower core body temperature. There was no significant difference in food intake or activity. Histological analyses demonstrated increased BAT lipid accumulation and hepatic steatosis in SMRT^{mRID1} mice (Figure 6E). There was no difference in WAT morphology (Figure S3A). These data indicate that mitochondrial function is a main target of SMRT in developing metabolic disorders.

Increased Susceptibility to Oxidative Stress in SMRT^{mRID1} Mice

Oxidative damage and diminished mitochondrial function contribute to the process of aging (Balaban et al., 2005). A common observation across different species is that the sensitivity to oxidative stress inversely correlates with life span (Kapahi et al., 1999; Kenyon, 2005). To determine the stress response, we challenged WT and SMRT^{mRID1} primary MEFs with hydrogen peroxide (H_2O_2) and assayed cell viability after 24 hr. SMRT^{mRID1} cells were more sensitive to oxidative damage and exhibited decreased survival at a lower H_2O_2 concentration than WT cells (Figure 7A), which was accompanied by increased ROS production (Figure 7B). Similar results were obtained with paraquat treatment (an ROS producing agent) (Figure 7C). The decreased stress resistance correlated with reduced expression of antioxidant genes (Figure 7D). Furthermore, a 2-fold increase in SMRT expression achieved by transient transfection in HepG2 cells (a human hepatoma cell line) was sufficient to reduce antioxidant gene expression and decrease survival upon H_2O_2 treatment (Figures 7E and S4A). Downregulation of *Catalase*, *Gpx1* and *Sod1* in WAT, *Gstp1* and *Gpx1* in muscle (Figure 7F), and *Catalase* in BAT (data not shown) was also found in SMRT^{mRID1} mice. Oxidative damage is believed to mediate cellular senescence (Colavitti and Finkel, 2005), which could be assessed by senescence-associated β-galactosidase (SA-β-gal) activity. By passage 10–12, many SMRT^{mRID1} MEFs exhibited an enlarged flattened morphology, which stained positive for SA-β-gal (Figure 7G, blue cell), whereas WT MEFs remained mostly β-gal negative. A similar increase in the SA-β-gal activity was detected in WAT from SMRT^{mRID1} mice (Figure 7G, bottom panel). To provide causative evidence for the described defect, MEFs were pretreated with PPARδ ligand for 60 hr, which increased stress resistance in SMRT^{mRID1} MEFs (Figure 7H). PPARδ ligand treatment upregulated *Mcad*, *Catalase*, *Gpx1*, and *Sod1* in WT and, to a lesser extent, in SMRT^{mRID1} cells, whereas PPARδ$^{-/-}$ MEFs exhibited increased susceptibility to oxidative damage similar to that in SMRT^{mRID1} MEFs (Figures S4B and S4C), suggesting that SMRT repression of PPARδ activity may contribute to the reduced oxidative resistance. Pretreatment with N-acetylcysteine (NAC), an antioxidant, for

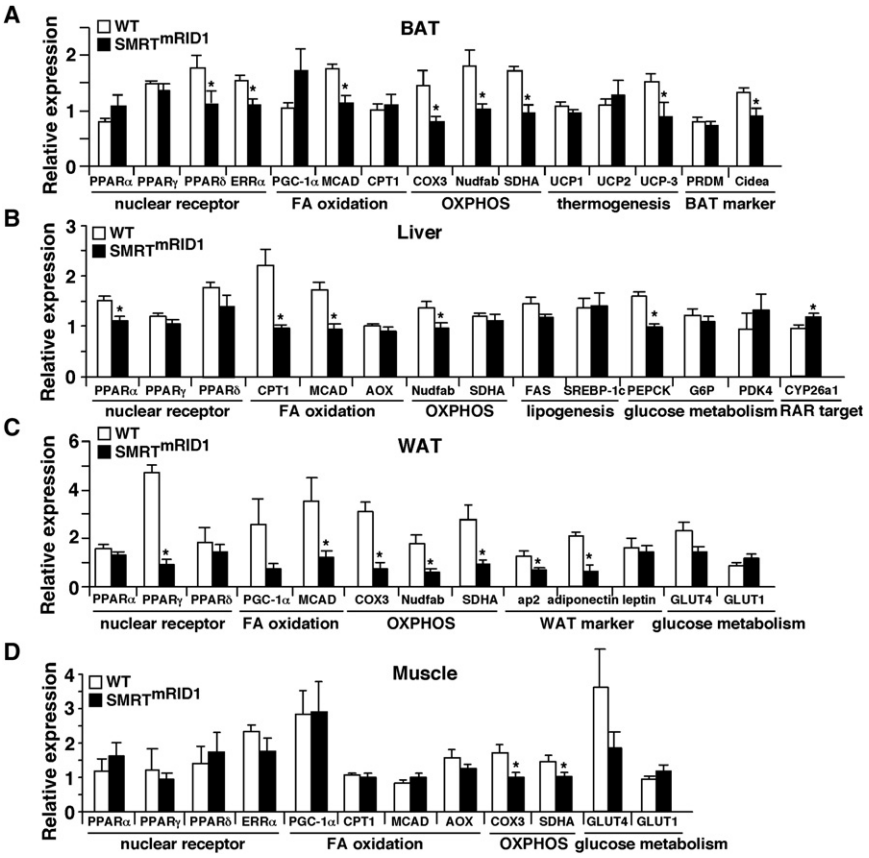

Figure 4. Suppressed Fatty Acid Oxidation and Oxidative Metabolism in SMRT^{mRID1} Mice

(A–D) Gene expression profiling by real-time PCR of brown adipose tissue (BAT), liver, white adipose tissue (WAT), and muscle from WT and SMRT^{mRID1} female mice on normal chow (6 months old, n = 6/genotype) after 5 hr fasting. OXPHOS: oxidative phosphorylation. Values are expressed as means ± SEM. *p < 0.05, comparing WT to SMRT^{mRID1} mice.

1 hr also completely rescued the phenotype of SMRT^{mRID1} MEFs (Figure 7I). In addition, NAC normalized the insulin response of SMRT^{mRID1} mice in ITT (Figure 7J). These results establish a link between suppressed mitochondrial function, decreased stress resistance, and age-related deterioration by SMRT^{mRID1}.

SMRT and Human Diseases

The human *Smrt* (*N-cor2*) gene is located on chromosome 12. We conducted preliminary analyses to examine potential associations of single-nucleotide polymorphisms (SNPs) in the human *Smrt* gene with either the risk of type 2 diabetes (T2D) or the level of high-molecular-weight (HMW) adiponectin, an adipokine that controls glucose and lipid homeostasis. Genotyping was conducted for 2745 patients with T2D and 3148 healthy controls (2422 males and 3221 females) from the Nurses' Health Study (NHS) and Health Professionals Follow-Up Study (HPFS). After adjusting for age and body mass index, we found a major cluster of SNPs within intron 1 of the human *Smrt* gene that were nominally associated with T2D (Figure 7K and Table S1). Clusters of SNPs associated with adiponectin levels (NHS only) could be found in intron 1, introns 15 and 16 (next to exons encoding SANT domain 2), and introns close to the C terminus of *Smrt* gene, where exons encoding RIDs are located (Figure 7K and Table S2). In line

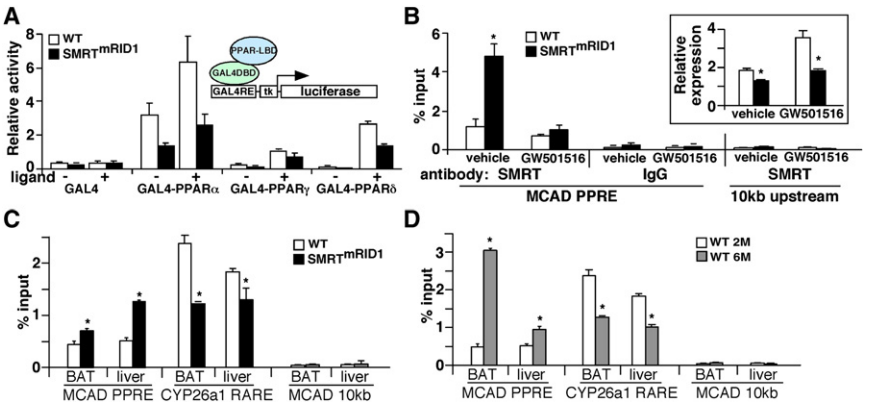

Figure 5. Assessment of PPAR Signaling in SMRT^{mRID1} Mice

(A) The transactivation activities of PPARs are suppressed in SMRT^{mRID1} primary preadipocytes derived from WAT. Preadipocytes/fibroblasts were isolated from the stromal vascular fraction of white fats. GAL4-DBD-PPAR-LBD constructs were transfected with a GAL4-luciferase reporter into these cells ± ligands. GAL4-DBD alone was included as a control. Ligand concentrations: GW7647 (PPARα), 1 μM; GW1929 (PPARγ), 1 μM; GW501516 (PPARδ), 0.1 μM.

(B) SMRT^{mRID1} reduces PPAR activity on target gene promoter. Chromatin immunoprecipitation (ChIP) was conducted in primary MEFs using antibody against SMRT or IgG as a control. SMRT occupancy on endogenous *Mcad* promoter was determined by real-time PCR using a primer set flanking the PPAR response element (PPRE). A control primer set amplifying a region 10 kb upstream of the *Mcad* gene was included as a negative control. Insert: The expression of *Mcad* mRNA in WT and SMRT^{mRID1} MEFs ± GW501516 (PPARδ ligand) was determined by real-time PCR.

(C) SMRT occupancy on target gene promoter in WT and SMRT^{mRID1} mice. Brown adipose tissue (BAT) and liver samples were collected from 2-month-old mice (n = 3/genotype) for ChIP using anti-SMRT antibody. SMRT binding to *Mcad* PPRE or *Cyp26a1* RARE (RAR target) was determined by real-time PCR.

(D) SMRT occupancy on target gene promoter in 2- month-old (2M) and 6-month-old (6M) mice determined by ChIP. Values are expressed as means ± SEM. *p < 0.05, comparing WT to SMRT^{mRID1} mice/cells or 2M to 6M.

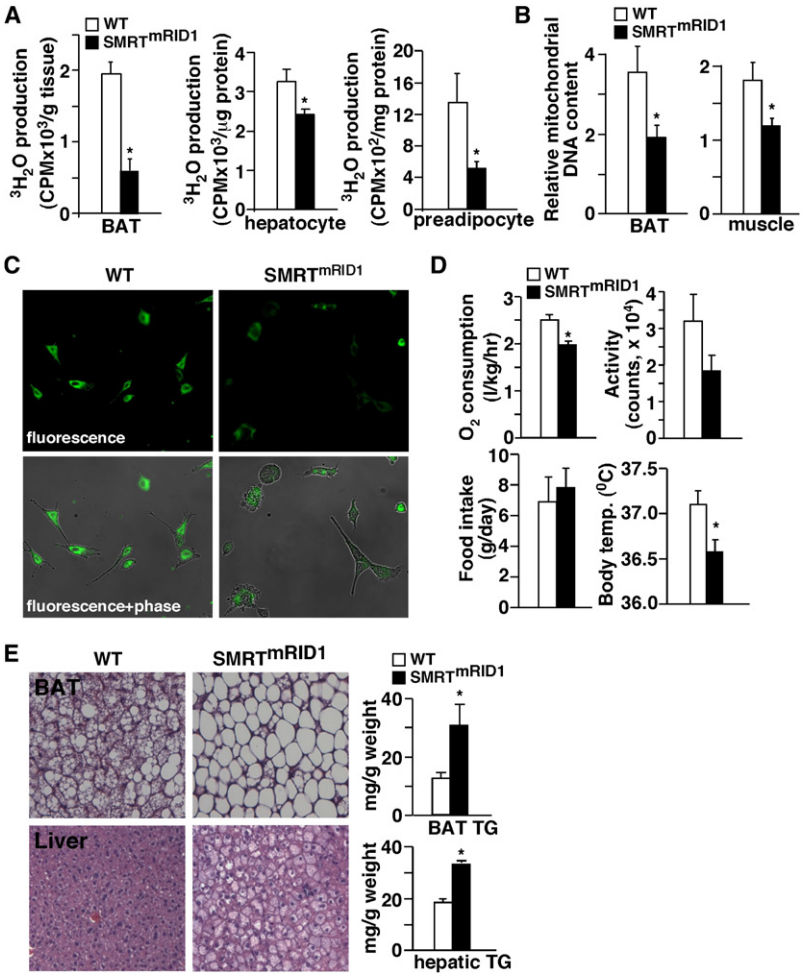

Figure 6. SMRT^{mRID1} Inhibits Mitochondrial Function

(A) Assessment of fatty acid β oxidation in brown fat (BAT) organ culture, primary hepatocytes, and preadipocytes/fibroblasts. The rate of fatty acid oxidation was determined by ^{3}H-palmitate breakdown to $^{3}H_2O$.

(B) Assessment of mitochondrial DNA content in BAT and muscle. Mitochondrial DNA was quantified by real-time PCR and normalized to nuclear DNA content.

(C) SMRT^{mRID1} MEFs have reduced mitochondrial content. MitoTracker staining (green fluorescence) was conducted to determine mitochondrial content.

(D) SMRT^{mRID1} mice show reduced O_2 consumption and lowered body temperature. O_2 consumption, activity, and food intake were determined by metabolic cages.

(E) Histological analyses of BAT and liver sections (H&E staining) to examine lipid accumulation (see also Figure S3). Tissue triglyceride (TG) content was measured by enzymatic assays. Muscle, BAT, and preadipocytes were isolated from 6-month-old mice. Primary hepatocytes were from 2.5-month-old mice. Values are expressed as means ± SEM. *p < 0.05, comparing WT to SMRT^{mRID1} mice/cells.

with the SNP data, we found an increase in SMRT binding to the PPRE of *Adiponectin* promoter in SMRT^{mRID1} adipocytes (Figure 7L). In addition, adiponectin administration to normalize the circulating concentration in SMRT^{mRID1} mice reduced the blood glucose level to that of WT animals (Figure 7M). Adiponectin also reverted the increased glucose production phenotype in SMRT^{mRID1} primary hepatocytes (Figure S2E). These data suggest that *Adiponectin* is a potential target of SMRT.

DISCUSSION

In this study, we use SMRT^{mRID1} mice to investigate the effects of SMRT repression on RID2-associated NRs. SMRT^{mRID1} mice show depressed mitochondrial function, partly mediated by inhibition of PPAR activities. This defect is accompanied by increased sensitivity to oxidative damage, accelerated aging, and development of metabolic deterioration. The expression of SMRT is upregulated with age in tissues that normally have high OXPHOS, which is associated with increased SMRT occupancy on PPAR target gene promoters. The current work provides a potential mechanism through which SMRT reduces metabolic rate and mediates age-related metabolic diseases.

The specificity of SMRT/NR interaction is determined by RID1/2, together with the third RID (upstream of the two RIDs) and splice variants lacking RID2. Our data indicate that when RID1 was mutated, PPAR/SMRT association was greatly enhanced (Figure 1D), indicating that RID1/2 and NR interaction is competitive. However, this competition mode is specific, as RID1 mutation did not affect TR/RID2 interaction. Interestingly, ChIP results suggest a switch of SMRT utilization from RID1-dependent to RID2-dependent NRs with age, as demonstrated by promoter occupancy of the *Cyp26a1* RARE and *Mcad* PPRE. It has been shown that the expression of *Rars* is reduced by aging (Pallet et al., 1997), which may be responsible for the reduced SMRT recruitment to the *Cyp26a1* promoter and may increase SMRT availability for PPARs. The SMRT^{mRID1} mouse model mimics this switch and, as such, offers a unique opportunity to distinguish the pathways regulated by RID2 involved in age-related pathophysiology. Several mouse models have been generated to examine the function of SMRT and N-CoR in NR function, including N-CoR point mutations, which abolished HDAC3 recruitment and exhibited defects in circadian clock gene expression controlled by Rev-erbα (Alenghat et al., 2008), and conditional deletion of the region containing RID1 and the third RID of N-CoR in the liver, which led to dysregulated thyroid hormone action (Astapova et al., 2008). Point mutations that abolished both RID1 and RID2 interaction of SMRT in mice (SMRT^{mRID} mice in a mixed C57BL/6 and sv129 background) also showed abnormal TR signaling and the associated metabolic defects (Nofsinger et al., 2008). These mice had increased fat-to-body weight ratio caused by uncontrolled PPARγ activation, although they gained significantly less weight. Using stable MEFs derived from WT, SMRT^{mRID1}, or SMRT^{mRID} mice in the mixed background, we also observed compromised antioxidant defense capacity in

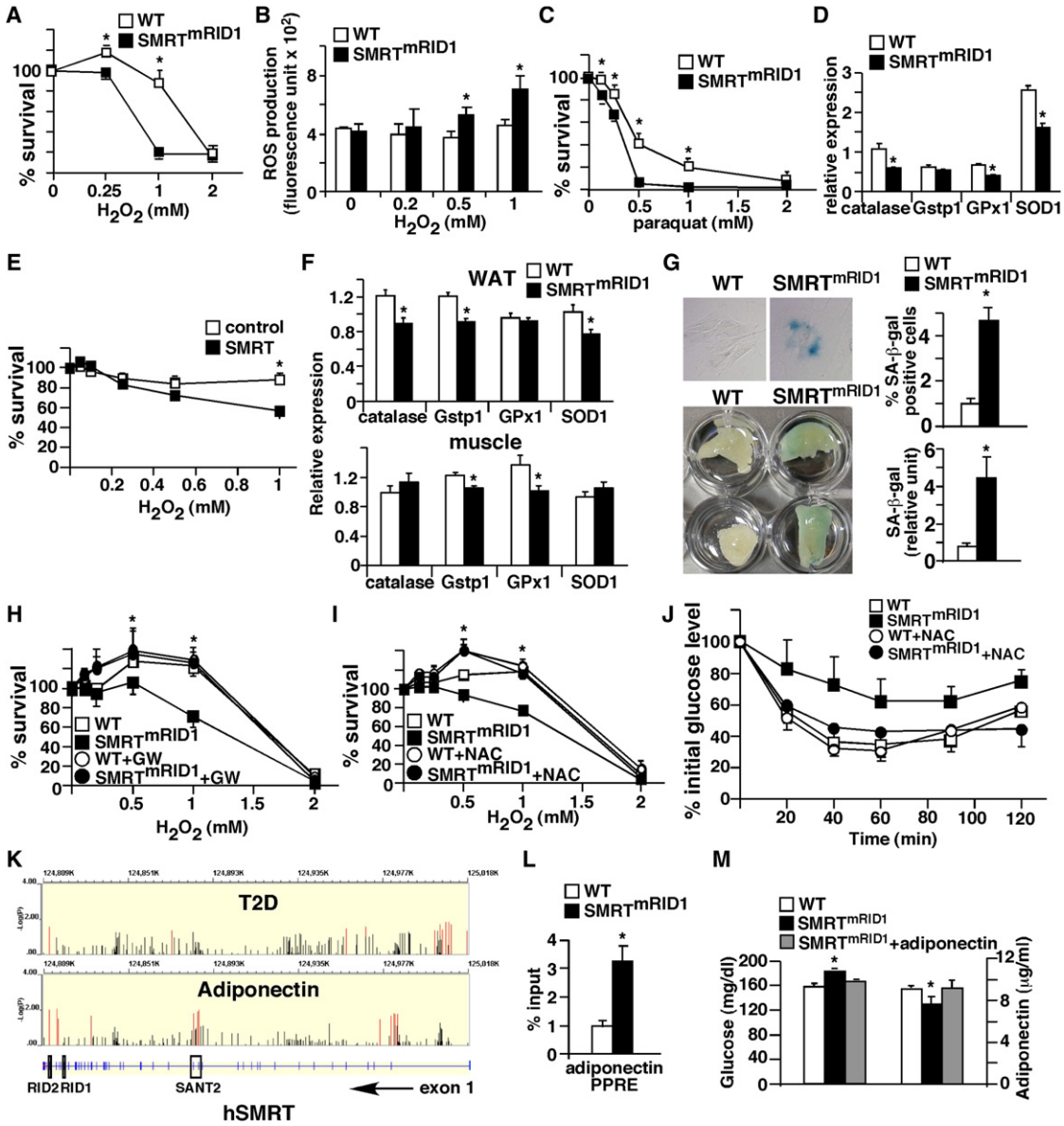

Figure 7. Increased Susceptibility to Oxidative Damage and Premature Senescence in SMRT^{mRID1} Cells

(A) Increased susceptibility to oxidative stress in SMRT^{mRID1} primary MEFs. WT and SMRT^{mRID1} MEFs were treated with H_2O_2 to induce oxidative stress, and cell survival was determined 24 hr later.

(B) Elevated ROS production in SMRT^{mRID1} MEFs determined by CM-H_2DCFDA.

(C) SMRT^{mRID1} MEFs exhibit reduced survival upon paraquat treatment.

(D) Downregulation of antioxidant genes in SMRT^{mRID1} MEFs determined by real-time PCR.

(E) SMRT overexpression reduces stress resistance in HepG2 cells. HepG2 cells were transfected with either the empty vector (control) or SMRT expression vector to achieve a 2-fold increase in *Smrt* mRNA levels (see Figure S4A). H_2O_2 treatment started 24 hr after transfection.

(F) Reduced tissue expression of genes encoding antioxidant defense mechanism in SMRT^{mRID1} mice determined by real-time PCR.

(G) SMRT^{mRID1} cells show premature senescence. Top: WT and SMRT^{mRID1} MEFs at passage 12 were stained with X-gal to examine senescence-associated β-galactosidase (SA-β-gal) activity (blue cells). Bottom: SA-β-gal activity in white adipose tissues from 6-month-old mice. The blue staining in tissue lysate was quantified and normalized to protein concentration.

(H) PPARδ activation rescues the phenotype of oxidative stress response in SMRT^{mRID1} cells. PPARδ ligand pretreatment (0.1 μM GW501516 for 60 hr) increased the survival of SMRT^{mRID1} cells.

(I) Antioxidant pretreatment normalizes the stress resistance of SMRT^{mRID1} MEFs. Cells were treated with 0.5 mM N-acetylcysteine (NAC, an antioxidant) 1 hr before H_2O_2 treatment.

(J) Insulin tolerance test showing NAC treatment reverts the reduced insulin response in SMRT^{mRID1} mice. NAC (10 mg/ml) was given in drinking water for 1 week. The difference between WT and SMRT^{mRID1} mice (n = 5/genotype, 6- to 8-month-old females) for each time point without NAC treatment was statistically significant (not significant after treatment).

SMRT^{mRID1} cells (Figures S3C–S3E). While we confirmed that SMRT^{mRID} MEFs had increased PPARγ activity, their ability to handle oxidative stress was comparable to WT cells. It is not unexpected that SMRT^{mRID} MEFs did not outperform WT cells in stress resistance, as PPARδ activation (or NAC treatment) did not shift the survival curve in WT MEFs. These two models therefore provide in vivo evidence supporting a specific role of RID2 for PPAR function. The current SMRT^{mRID1} mouse study reveals that shifting SMRT repression to increase RID2-mediated interaction to receptors like PPARs results in accelerated aging and metabolic syndrome.

Both *Smrt* and *N-cor* whole-body knockout mice are embryonic lethal, indicating nonredundant functions for these corepressors (Ghisletti et al., 2009; Hermanson et al., 2002; Jepsen et al., 2007). Our data demonstrate age-dependent upregulation of *N-cor* mRNA in the liver (Figure S1A) and *Smrt* mRNA in muscle and BAT, both of which play important roles in fat burning and oxidative metabolism. At the protein level, SMRT is increased in WAT, in addition to BAT and muscle in older animals. Although SMRT expression in the liver remains unchanged in older mice, there is also more hepatic SMRT binding to *Mcad* PPRE with age. These observations implicate a multitier regulation of SMRT activity by aging and predict a role for SMRT in major metabolic tissues. In fact, transcriptional programs encoding OXPHOS and fatty acid catabolism pathways are downregulated in most of these tissues in SMRT^{mRID1} mice. We attribute this phenotype to increased suppression of PPAR activities by the mutant SMRT protein, as PPARs are major regulators of oxidative metabolism and the expression of *Pparδ*, *Pparα*, and *Pparγ* was downregulated in BAT, liver, and WAT of SMRT^{mRID1} mice, respectively. In M2 interaction and ChIP assays, SMRT^{mRID1} and PPAR association was enhanced. As a result, the transactivation activities of PPARs were reduced in primary cells isolated from SMRT^{mRID1} mice. The adipogenic potential of SMRT^{mRID1} preadipocytes was only moderately affected, possibly due to the fact that the inhibition of PPARγ activity was partial and levels of other adipogenic transcriptional factors, including *C/ebpβ* and *C/ebpδ*, remained similar (Figure S3B). Accordingly, the obesity phenotype of SMRT^{mRID1} mice is likely mediated by reduced mitochondrial metabolic capacity. Of note, under unchallenged conditions, the hearts of SMRT^{mRID1} mice appeared morphologically normal and the expression pattern of OXPHOS was mostly unaltered (except for a reduction in *Gpx1* [Figure S2D]), suggesting that SMRT is less critical in this tissue. We cannot rule out the possibility that other potential RID2-associated NRs, such as ERRα, may contribute to the deregulated mitochondrial function. However, ERRα and SMRT do not interact in vitro (data not shown). Derepression of RID1-associated NRs, such as RARs, could also contribute to the phenotype. Although the role of RA signaling in metabolism is less defined, it has been shown that retinaldehyde, the precursor of RA, modulates metabolic homeostasis partly by suppressing PPARγ responses (Ziouzenkova et al., 2007). Therefore, dysregulated RA/RAR activities could also have an impact on PPAR-mediated regulation. Interestingly, RAR signaling in embryonic development seems to be unaffected in SMRT^{mRID1} mice, probably because the RID1 mutation does not completely abolish RAR/SMRT interaction and/or because N-CoR provides sufficient repression function. Regardless, these results demonstrate a function for SMRT in the control of oxidative metabolism.

Although assessment of stress resistance in MEFs is one of the standard approaches for aging studies, the limitation of such an assay is that it provides correlative results. It is also possible that the observed mitochondrial dysfunction is a consequence of metabolic defects. However, several lines of evidence indicate that SMRT suppression of mitochondrial function and the antioxidant defense mechanism accelerates aging and related metabolic diseases. SMRT overexpression in HepG2 cells was sufficient to reduce antioxidant gene expression and stress resistance, whereas NAC treatment normalized the stress and insulin responses in SMRT^{mRID1} MEFs and mice, respectively. In addition, PPARδ activation, which enhanced mitochondrial function, also rescued the phenotype of increased sensitivity to oxidative damage in SMRT^{mRID1} MEFs. Population-based studies further demonstrate nominal association of human *Smrt* gene SNPs with T2D and levels of adiponectin. *Adiponectin* is a PPARγ target gene known to regulate mitochondrial function and metabolism through activation of AMP-activated kinase (AMPK) (Kadowaki and Yamauchi, 2005; Kahn et al., 2005). AMPK has also been shown to control longevity in *C. elegans* (Greer et al., 2009). Most of the SNPs are located in intron 1 and introns close to exons encoding SANT domain 2 and RIDs. These SNPs may modify the expression and/or splicing of *Smrt*, which are expected to affect the suppressive activity and NR interacting preference. Additional work will be required to determine the functional relevance of these SNPs in human *Smrt* gene to define the relationship between SMRT, age-related decline in mitochondrial function, and human diseases. The current study establishes a molecular basis for designing therapeutic approaches that release SMRT RID2-mediated repression, such as PPARδ agonists, to increase the mitochondrial integrity and reduce oxidative stress. Future work aiming to identify pathways that upregulate (or downregulate) SMRT and examine the interaction between dietary fats, PPARs, and SMRT will further provide insights into drug discovery to improve health span.

(K) The associations of SNPs in human *Smrt* (*N-cor*) gene with the risk of type 2 diabetes (T2D) and plasma high-molecular-weight (HMW) adiponectin concentration, annotated with the gene structure (bottom panel: exons are shown). The y axis represents −log(p value) from the logistic regression (T2D) and linear regression (HMW adiponectin) analyses. All identified SNPs are shown. The red lines represent the associations of nominal significance (p value < 0.05) (see also Tables S1 and S2).

(L) ChIP showing increased SMRT binding on the PPRE of *Adiponectin* promoter in SMRT^{mRID1} adipocytes. Primary adipocytes were isolated from 2-month-old mice. IgG ChIP or 10k b upstream negative controls showed no specific bindings (data not shown).

(M) Adiponectin administration normalizes the glucose level in SMRT^{mRID1} mice. Tail vein injection of 10 μg recombinant adiponectin in SMRT^{mRID1} mice increased the serum adiponectin level similar to that in WT mice (shown on the right), which normalized the blood glucose concentration (shown on the left). Values are expressed as means ± SEM. *p < 0.05, comparing WT to SMRT^{mRID1} mice/cells.

EXPERIMENTAL PROCEDURES

SMRT^{mRID1} Mice and Metabolic Studies

SMRT^{mRID1} mice were provided by Ronald M. Evans at the Salk Institute and were generated similarly to SMRT^{mRID} mice (mutations in both RID1 and RID2) in a mixed background (50% sv129 and 50% C57BL/6) as described previously (Nofsinger et al., 2008). The detailed methodology of SMRT^{mRID1} mouse generation will be reported elsewhere. They were backcrossed two generations to the C57BL/6 background (87.5%). Heterozygous mice were mated to create cohorts of age-matched WT and SMRT^{mRID1} mice. Six-month-old female and male mice were used to assess metabolic capacity after 5 hr fast. Experiments were repeated and data were collected from multiple cohorts (n = 5–8/cohort/genotype). GTT was performed by intraperitoneal (i.p.) injection of 1.5 g glucose/kg body weight, and ITT was conducted using 1 U insulin/kg. Recombinant adiponectin protein (AXXORA, LLC) was administered through tail vein (10 μg), and blood samples were collected 1 hr later for glucose and adiponectin concentration analyses. Control PBS injection had no effect. Tissue-specific insulin signaling was determined by i.p. injection of 2 U insulin/kg or control saline. Tissues were collected 15 min later for determining insulin-stimulated Akt phosphorylation using anti-Ser473 Akt antibody (Cell Signaling). Serum hormones were measured using commercial ELISA kits (R&D Systems, Millipore, and Cayman Chemicals). Metabolic cage studies were performed using a monitoring system from Columbus Instruments. Sensorimotor coordination was assayed with a fixed-speed Rotarod (4 rpm). Statistics analyses were performed using Student's t test (two-tailed), except for survival curves, which were determined using the Mantel-Haenszel log rank test. All mice were housed in a barrier facility, fed normal chow, and kept on a 12 hr light/12 hr dark cycle. Animal studies were approved by the Harvard Medical Area Standing Committee on Animals.

Primary Cells and In Vitro Assays

Hepatocytes were isolated by portal vein perfusion with blendzyme (Roche) and cultured in William's Medium E with 5% FBS. Primary preadipocytes/fibroblasts were derived from the stromal vascular fraction of WAT after collagenase digestion. The rate of fatty acid β oxidation was determined by measuring ^{3}H-palmitate breakdown to ^3H_2O. The glucose uptake assay was conducted using 2-^{3}H-deoxy-D-glucose in Krebs-Ringer bicarbonate HEPES buffer ± 100 nM insulin. MEFs were isolated from e15 embryos. For the oxidative stress assays, MEFs (or HepG2 cells) were plated to confluence and allowed to attach overnight. H_2O_2 or paraquat was added to the indicated final concentration, and the cells were incubated for another 24 hr. NAC (0.5 mM) was added for 1 hr and removed prior to H_2O_2 treatment. To examine the ligand effect, cells were plated in media ± 0.1 μM GW501516 for 60 hr before H_2O_2 treatment. Cell survival was assayed using the ATP bioluminescent somatic cell assay kit (Sigma-Aldrich). ROS production was determined by incubating MEFs ± 5 μM CM-H_2DCFDA (Invitrogen) for 30 min. Fluorescence units were measured and normalized to protein concentration. ChIP of early-passage MEFs or tissues was performed using the SimpleChIP Enzymatic Chromatin IP kit (Cell Signaling). The primer pair used for real-time PCR was based on the reported PPRE on mouse *Mcad* (Gulick et al., 1994) or *Adiponectin* promoter (Iwaki et al., 2003). A second pair located 10 kb upstream of the *Mcad/Adiponectin* gene was included as a negative control. The primers for RARE on mouse *CYP26a1* promoter were described previously (Loudig et al., 2000). Anti-SMRT antibody was from Santa Cruz Biotechnology.

Mitochondrial DNA Content, Gene Expression, Transient Transfection, and SNP Analysis

Relative mitochondrial DNA and nuclear DNA levels were determined using real-time PCR primers specific to mitochondrial gene NADH dehydrogenase subunit 1 (*Nd1*) and genomic gene *36B4*. RNA was reverse transcribed with oligo-dT and random hexamer primers (Thermo Scientific), and gene expression was determined by SYBR Green-based real-time PCR using *36B4* for normalization. The expression in human HepG2 cells was normalized to *18S*. To determine SMRT protein levels, tissue lysates were subjected to immunoprecipitation with anti-SMRT antibody (Santa Cruz Biotechnology), followed by immunoblotting (Figures S1B and S1E). For normalization, actin levels in the input were determined. Quantification was performed using ImageJ. The mammalian two-hybrid assay was conducted in AD293 cells cultured in dialyzed FBS depleted of steroid/nonsteroid hormones and lipoproteins to reduce NR ligands in the media. Luciferase activities were determined 48 hr after transfection using the Dual-Luciferase System (Promega). HepG2 cells were transfected with control or SMRT expression vectors 24 hr prior to the oxidative stress assay. All of the expression vectors were under the control of a CMV promoter. The populations, data collection, and statistical analyses for human *Smrt* gene SNPs are described in the Supplemental Information.

SUPPLEMENTAL INFORMATION

Supplemental Information includes Supplemental Experimental Procedures, Supplemental References, four figures, and two tables and can be found with this article online at doi:10.1016/j.cmet.2010.11.007.

ACKNOWLEDGMENTS

We thank James Mitchell and Wei Xu for valuable comments and Gokhan Hotamisligil (Harvard School of Public Health) for assistance in metabolic cages and DEXA experiments. S.M.R. was supported by NIEHS training grants (T32ES07155 and T32ES016645). P.B. was supported by NIDDK training grants (T90DK070078 and T32ES016645). This work was supported by the Howard Hughes Medical Institute, the Glenn Foundation, the Helmsley Foundation, and NIH grants 5R37DK057978 and 5 R01HD027183 (R.M.E); by the American Heart Association, Boston Obesity Nutrition Research Center (DK46200), and NIH grant R01HL71981 (L.Q.); by NIH grants DK58845 and U01HG004399 (F.B.H); and by the American Heart Association, American Diabetes Association, and NIH grant R01DK075046 (C.-H.L.).

Received: January 9, 2010
Revised: July 10, 2010
Accepted: October 12, 2010
Published: November 30, 2010

REFERENCES

Alenghat, T., Meyers, K., Mullican, S.E., Leitner, K., Adeniji-Adele, A., Avila, J., Bućan, M., Ahima, R.S., Kaestner, K.H., and Lazar, M.A. (2008). Nuclear receptor corepressor and histone deacetylase 3 govern circadian metabolic physiology. Nature *456*, 997–1000.

Astapova, I., Lee, L.J., Morales, C., Tauber, S., Bilban, M., and Hollenberg, A.N. (2008). The nuclear corepressor, NCoR, regulates thyroid hormone action in vivo. Proc. Natl. Acad. Sci. USA *105*, 19544–19549.

Balaban, R.S., Nemoto, S., and Finkel, T. (2005). Mitochondria, oxidants, and aging. Cell *120*, 483–495.

Baur, J.A., Pearson, K.J., Price, N.L., Jamieson, H.A., Lerin, C., Kalra, A., Prabhu, V.V., Allard, J.S., Lopez-Lluch, G., Lewis, K., et al. (2006). Resveratrol improves health and survival of mice on a high-calorie diet. Nature *444*, 337–342.

Cohen, R.N., Brzostek, S., Kim, B., Chorev, M., Wondisford, F.E., and Hollenberg, A.N. (2001). The specificity of interactions between nuclear hormone receptors and corepressors is mediated by distinct amino acid sequences within the interacting domains. Mol. Endocrinol. *15*, 1049–1061.

Colavitti, R., and Finkel, T. (2005). Reactive oxygen species as mediators of cellular senescence. IUBMB Life *57*, 277–281.

Ghisletti, S., Huang, W., Jepsen, K., Benner, C., Hardiman, G., Rosenfeld, M.G., and Glass, C.K. (2009). Cooperative NCoR/SMRT interactions establish a corepressor-based strategy for integration of inflammatory and anti-inflammatory signaling pathways. Genes Dev. *23*, 681–693.

Glass, C.K., and Rosenfeld, M.G. (2000). The coregulator exchange in transcriptional functions of nuclear receptors. Genes Dev. *14*, 121–141.

Greer, E.L., Banko, M.R., and Brunet, A. (2009). AMP-activated protein kinase and FoxO transcription factors in dietary restriction-induced longevity. Ann. N. Y. Acad. Sci. *1170*, 688–692.

Guarente, L. (2006). Sirtuins as potential targets for metabolic syndrome. Nature *444*, 868–874.

Gulick, T., Cresci, S., Caira, T., Moore, D.D., and Kelly, D.P. (1994). The peroxisome proliferator-activated receptor regulates mitochondrial fatty acid oxidative enzyme gene expression. Proc. Natl. Acad. Sci. USA *91*, 11012–11016.

Hermanson, O., Jepsen, K., and Rosenfeld, M.G. (2002). N-CoR controls differentiation of neural stem cells into astrocytes. Nature *419*, 934–939.

Houstis, N., Rosen, E.D., and Lander, E.S. (2006). Reactive oxygen species have a causal role in multiple forms of insulin resistance. Nature *440*, 944–948.

Hu, X., Li, Y., and Lazar, M.A. (2001). Determinants of CoRNR-dependent repression complex assembly on nuclear hormone receptors. Mol. Cell. Biol. *21*, 1747–1758.

Hu, X., Li, S., Wu, J., Xia, C., and Lala, D.S. (2003). Liver X receptors interact with corepressors to regulate gene expression. Mol. Endocrinol. *17*, 1019–1026.

Iwaki, M., Matsuda, M., Maeda, N., Funahashi, T., Matsuzawa, Y., Makishima, M., and Shimomura, I. (2003). Induction of adiponectin, a fat-derived antidiabetic and antiatherogenic factor, by nuclear receptors. Diabetes *52*, 1655–1663.

Jepsen, K., Solum, D., Zhou, T., McEvilly, R.J., Kim, H.J., Glass, C.K., Hermanson, O., and Rosenfeld, M.G. (2007). SMRT-mediated repression of an H3K27 demethylase in progression from neural stem cell to neuron. Nature *450*, 415–419.

Kadowaki, T., and Yamauchi, T. (2005). Adiponectin and adiponectin receptors. Endocr. Rev. *26*, 439–451.

Kahn, B.B., Alquier, T., Carling, D., and Hardie, D.G. (2005). AMP-activated protein kinase: ancient energy gauge provides clues to modern understanding of metabolism. Cell Metab. *1*, 15–25.

Kang, K., Reilly, S.M., Karabacak, V., Gangl, M.R., Fitzgerald, K., Hatano, B., and Lee, C.H. (2008). Adipocyte-derived Th2 cytokines and myeloid PPARdelta regulate macrophage polarization and insulin sensitivity. Cell Metab. *7*, 485–495.

Kapahi, P., Boulton, M.E., and Kirkwood, T.B. (1999). Positive correlation between mammalian life span and cellular resistance to stress. Free Radic. Biol. Med. *26*, 495–500.

Kenyon, C. (2005). The plasticity of aging: insights from long-lived mutants. Cell *120*, 449–460.

Lagouge, M., Argmann, C., Gerhart-Hines, Z., Meziane, H., Lerin, C., Daussin, F., Messadeq, N., Milne, J., Lambert, P., Elliott, P., et al. (2006). Resveratrol improves mitochondrial function and protects against metabolic disease by activating SIRT1 and PGC-1alpha. Cell *127*, 1109–1122.

Lee, C.H., Olson, P., and Evans, R.M. (2003). Minireview: lipid metabolism, metabolic diseases, and peroxisome proliferator-activated receptors. Endocrinology *144*, 2201–2207.

Lee, S.J., Murphy, C.T., and Kenyon, C. (2009). Glucose shortens the life span of C. elegans by downregulating DAF-16/FOXO activity and aquaporin gene expression. Cell Metab. *10*, 379–391.

Lin, J., Handschin, C., and Spiegelman, B.M. (2005). Metabolic control through the PGC-1 family of transcription coactivators. Cell Metab. *1*, 361–370.

Loudig, O., Babichuk, C., White, J., Abu-Abed, S., Mueller, C., and Petkovich, M. (2000). Cytochrome P450RAI(CYP26) promoter: a distinct composite retinoic acid response element underlies the complex regulation of retinoic acid metabolism. Mol. Endocrinol. *14*, 1483–1497.

Murphy, C.T., McCarroll, S.A., Bargmann, C.I., Fraser, A., Kamath, R.S., Ahringer, J., Li, H., and Kenyon, C. (2003). Genes that act downstream of DAF-16 to influence the lifespan of Caenorhabditis elegans. Nature *424*, 277–283.

Nofsinger, R.R., Li, P., Hong, S.H., Jonker, J.W., Barish, G.D., Ying, H., Cheng, S.Y., Leblanc, M., Xu, W., Pei, L., et al. (2008). SMRT repression of nuclear receptors controls the adipogenic set point and metabolic homeostasis. Proc. Natl. Acad. Sci. USA *105*, 20021–20026.

Pallet, V., Azaïs-Braesco, V., Enderlin, V., Grolier, P., Noël-Suberville, C., Garcin, H., and Higueret, P. (1997). Aging decreases retinoic acid and triiodothyronine nuclear expression in rat liver: exogenous retinol and retinoic acid differentially modulate this decreased expression. Mech. Ageing Dev. *99*, 123–136.

Pan, D., Fujimoto, M., Lopes, A., and Wang, Y.X. (2009). Twist-1 is a PPARdelta-inducible, negative-feedback regulator of PGC-1alpha in brown fat metabolism. Cell *137*, 73–86.

Privalsky, M.L. (2004). The role of corepressors in transcriptional regulation by nuclear hormone receptors. Annu. Rev. Physiol. *66*, 315–360.

Reilly, S.M., and Lee, C.H. (2008). PPAR delta as a therapeutic target in metabolic disease. FEBS Lett. *582*, 26–31.

Reznick, R.M., Zong, H., Li, J., Morino, K., Moore, I.K., Yu, H.J., Liu, Z.X., Dong, J., Mustard, K.J., Hawley, S.A., et al. (2007). Aging-associated reductions in AMP-activated protein kinase activity and mitochondrial biogenesis. Cell Metab. *5*, 151–156.

Roberts, C.K., and Sindhu, K.K. (2009). Oxidative stress and metabolic syndrome. Life Sci. *84*, 705–712.

Rodgers, J.T., Lerin, C., Haas, W., Gygi, S.P., Spiegelman, B.M., and Puigserver, P. (2005). Nutrient control of glucose homeostasis through a complex of PGC-1alpha and SIRT1. Nature *434*, 113–118.

St-Pierre, J., Drori, S., Uldry, M., Silvaggi, J.M., Rhee, J., Jäger, S., Handschin, C., Zheng, K., Lin, J., Yang, W., et al. (2006). Suppression of reactive oxygen species and neurodegeneration by the PGC-1 transcriptional coactivators. Cell *127*, 397–408.

Wallace, D.C., and Fan, W. (2009). The pathophysiology of mitochondrial disease as modeled in the mouse. Genes Dev. *23*, 1714–1736.

Wang, Y.X., Zhang, C.L., Yu, R.T., Cho, H.K., Nelson, M.C., Bayuga-Ocampo, C.R., Ham, J., Kang, H., and Evans, R.M. (2004). Regulation of muscle fiber type and running endurance by PPARdelta. PLoS Biol. *2*, e294.

Zid, B.M., Rogers, A.N., Katewa, S.D., Vargas, M.A., Kolipinski, M.C., Lu, T.A., Benzer, S., and Kapahi, P. (2009). 4E-BP extends lifespan upon dietary restriction by enhancing mitochondrial activity in Drosophila. Cell *139*, 149–160.

Ziouzenkova, O., Orasanu, G., Sharlach, M., Akiyama, T.E., Berger, J.P., Viereck, J., Hamilton, J.A., Tang, G., Dolnikowski, G.G., Vogel, S., et al. (2007). Retinaldehyde represses adipogenesis and diet-induced obesity. Nat. Med. *13*, 695–702.